SIAM J. IMAGING SCIENCES
Vol. 16, No. 2, pp. 948–968

Numerical Reconstruction of Radiative Sources from Partial Boundary Measurements*

Hiroshi Fujiwara†, Kamran Sadiq‡, and Alexandru Tamasan§

Abstract. We consider an inverse source problem in the stationary radiative transport through an absorbing and scattering medium in two dimensions. Using the angularly resolved radiation measured on an arc of the boundary, we propose a numerical algorithm to recover the source in the convex hull of this arc. The method involves an unstable step of inverting a bounded operator whose range is not closed. We show that the continuity constant of the discretized inverse grows at most linearly with the discretization step, thus stabilizing the problem. Numerical examples presented show the effectiveness of the proposed method.

Key words. radiative transport, source reconstruction, numerical solution to Cauchy type singular integral equations, A-analytic maps, Hilbert transform, Bukhgeim–Beltrami equation, optical molecular imaging

MSC codes. 65N21, 45E05

DOI. 10.1137/22M1507449

1. Introduction.

Let Ω be a two-dimensional convex domain with smooth boundary, let Λ be an arc on its boundary $\partial\Omega$, and let $\Omega^+ := \mathrm{Conv}(\Lambda) \cap \Omega$ be its convex hull inside Ω; see Figure 1. In the stationary case, when generated by a source of radiation q embedded in Ω, the density $I(z,\xi)$ of particles at $z \in \Omega$ moving in the direction $\xi \in S^1$ solves the radiative transport problem: for $(z,\xi) \in \Omega \times S^1$,

$$\xi \cdot \nabla_z I(z,\xi) + (\mu_{\mathrm{a}}(z) + \mu_{\mathrm{s}}(z)) I(z,\xi) - \mu_{\mathrm{s}}(z) \int_{S^1} p(z; \xi \cdot \xi') I(z,\xi') d\sigma_{\xi'} = q(z), \tag{1.1}$$

$$I(z,\xi)\,|_{\Gamma_-} = 0, \tag{1.2}$$

*Received by the editors July 5, 2022; accepted for publication (in revised form) December 13, 2022; published electronically June 7, 2023.
https://doi.org/10.1137/22M1507449
Funding: The work of the first author was supported by the JSPS KAKENHI grants JP20H01821, JP21H00999, and JP22K18674. The work of the second author was supported by the Austrian Science Fund (FWF) project P31053-N32 and by the FWF Project F6801-N36 within the Special Research Program SFB F68 "Tomography Across the Scales." The work of the third author was partially supported by the National Science Foundation grant DMS-1907097.

†Graduate School of Informatics, Kyoto University, Kyoto, 606-8501, Japan (fujiwara@acs.i.kyoto-u.ac.jp).
‡Johann Radon Institute of Computational and Applied Mathematics (RICAM), 4040 Linz, Austria, and Faculty of Mathematics, University of Vienna, 1090 Vienna, Austria (kamran.sadiq@ricam.oeaw.ac.at).
§Department of Mathematics, University of Central Florida, Orlando, FL 32816-1364 USA (tamasan@math.ucf.edu).

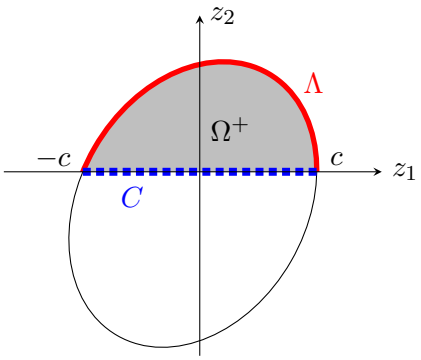

Figure 1. *Exiting radiation is measured only on* Λ.

where μ_a and μ_s are, respectively, the absorption and the scattering coefficients, and p is the scattering phase function. The latter represents the probability at which particles change direction from ξ' to ξ due to scattering at z. In particular, $\int_{S^1} p(z;\xi\cdot\xi')\,d\sigma_{\xi'} = 1$, with $d\sigma_{\xi'}$ denoting the arc element on S^1. In (1.2) we distinguish the inflow boundary $\Gamma_- = \{(z,\xi) \in \partial\Omega \times S^1\,;\, \nu(z)\cdot\xi < 0\}$, where $\nu(z)$ is the outer unit normal at $z \in \partial\Omega$. The boundary condition (1.2) indicates that no radiation enters the domain from outside Ω.

We are concerned with the following inverse source problem: Reconstruct the unknown internal isotropic source q in Ω^+ from measurement of the outflow $I|_{\Lambda_+}$ on Λ_+, where

$$\Lambda_+ = \{(z,\xi) \in \Lambda \times S^1\,;\, \nu(z)\cdot\xi > 0\}.$$

The medium (as characterized by μ_a, μ_s, and p) is assumed to be known.

The inverse source problem above has applications in medical imaging: In a nonscattering ($\mu_s = 0$) and nonattenuating ($\mu_a = 0$) medium the problem is mathematically equivalent to the one occurring in classical computerized X-ray tomography (e.g., [3, 14, 25], but note that q in (1.1) then encodes the absorbing property of the medium). In a nonscattering ($\mu_s = 0$), but attenuating medium ($\mu_a > 0$), such a problem appears in Positron/Single Photon Emission Tomography (PET/SPECT). For applications in scattering media ($\mu_s > 0$) the inverse source problem for (1.1) is the two-dimensional version of a problem in Optical Molecular Imaging [1, 18, 20] for cylindrical media when the optical properties and the source are constant in one direction.

If the exiting radiation is known on the entire boundary (case $\Lambda = \partial\Omega$), then q is uniquely determined in Ω as shown in [31] in the Euclidean domains, and in [29] on a simple Riemannian surface with small curvature. Theoretical reconstructions from complete boundary data have also been proposed in [2] in weakly scattering media and, for nonweakly scattering media in [4, 8, 9], see also [30] for slab domains and data on both sides of the boundary.

For the case where exiting radiation is known only on a part of the boundary, the singular support of the source can be recovered in a specific subdomain [15]. To the best of the authors' knowledge, there are no known results to quantitatively determine q in the entire domain Ω. However, the unique determination of the source $q|_{\Omega^+}$ from data on an arc of the boundary has been recently established by the authors in [10]. The reconstruction method is based on Bukhgeim's theory of A-analytic functions [3] and summarized in section 2. While

a classical spectral analysis argument in [10] showed the problem to be ill-posed, the naive implementation (regularization by discretization only) produced better than expected results.

Here we analyze the ill-posedness in the problem as it arises in the numerical algorithm and propose two regularized methods to effectively reconstruct q in Ω^+ from exiting radiation on Λ. In particular, Theorem 3.1 shows that the ill-posedness is not severe, thus explaining the preliminary reconstructions imaged in [10]. Different from [9], in here the data is given on a part of the boundary. We know of no other method for quantitative imaging of a radiative source in stationary radiative transport, where data is collected on one side of the boundary.

Key to the partial boundary data case is the uniqueness of solution to the Cauchy type singular integral equation (CSIE)

$$[I - bH_c]f(x) = \Phi(x), \quad -c < x < c, \tag{1.3}$$

where I is the identity operator, b is a complex parameter, and

$$H_c[f](x) = \frac{1}{\pi}\text{p.v.}\int_{-c}^{c} \frac{f(y)}{x-y}\,dy \tag{1.4}$$

is the finite Hilbert transform of functions on $(-c, c)$. Motivated by its applications to airfoil in aerodynamics and fracture mechanics in elasticity, numerous literature has studied CSIEs [5, 12, 13, 16, 24, 33] for the case $b \neq i$. However, our problem leads to consider (1.3) for $b = i$. It is known [21, 26] that the spectrum of iH_c on $L^2(-c, c)$ is the interval $[-1, 1]$. Fortunately, 1 is not in the point spectrum of iH_c [11, 35], thus allowing one to invert $(I - iH_c)$ in its range. Unfortunately, the range of $(I - iH_c)$ is a dense proper subset of $L^2(-c, c)$ yielding an unstable inversion with the discretization schemes rendered ill-conditioned. The spectrum analysis by itself does not shed light on how severe this ill-posedness can be.

In section 3 we analyze this ill-posedness in the case of the piecewise constant approximation, show unique solvability, and estimate a degree of ill-conditionedness of our discretization scheme.

In section 4 we formulate two numerical algorithms, which are implemented in the numerical experiments in section 5.

2. Preliminaries.

This section provides a brief summary of the theoretical method used in our numerical reconstruction. For details we refer to [10, 11] and references herein.

We use the identification of spatial points $z = (z_1, z_2) \in \mathbb{R}^2$ with their complex representation $z = z_1 + iz_2 \in \mathbb{C}$, and identify velocities $\xi \in S^1$ with $\theta \in \mathbb{R}/2\pi$ by the standard polar coordinate $\xi = (\cos\theta, \sin\theta)$. Derivatives $\partial = (\partial_{z_1} - i\partial_{z_2})/2$ and $\overline{\partial} = (\partial_{z_1} + i\partial_{z_2})/2$ convert the advection operator to $\xi \cdot \nabla_z = e^{-i\theta}\overline{\partial} + e^{i\theta}\partial$.

The exact solution I to the problem (1.1) and (1.2) has the Fourier expansion with respect to ξ in $L^2(S^1)$,

$$I(z, \xi(\theta)) = \sum_{m\in\mathbb{Z}} I_m(z)e^{im\theta}.$$

Our boundary data is equivalent to knowledge of the sequence $(I_m|_\Lambda\,;\, m \in \mathbb{Z})$ on Λ. Suppose that there exists a positive integer M such that p is sufficiently well approximated by its Fourier polynomial in the angular variable,

$$p(z;\xi\cdot\xi')\approx\sum_{|m|\le M}p_m(z)e^{im\theta},$$

where $\theta=\arccos(\xi\cdot\xi')$.

Since q is isotropic, and I is real-valued, the radiative transport equation (1.1) decomposes into the infinite elliptic system in Ω:

$$\overline{\partial}I_1+\partial I_{-1}+\mu_{\mathrm{t}}I_0=2\pi\mu_{\mathrm{s}}p_0I_0+q, \tag{2.1}$$

$$\overline{\partial}I_{-m}+\partial I_{-m-2}+\mu_{\mathrm{t}}I_{-m-1}=2\pi\mu_{\mathrm{s}}p_{-m-1}I_{-m-1}, \qquad 0\le m\le M-1, \tag{2.2}$$

$$\overline{\partial}I_{-m}+\partial I_{-m-2}+\mu_{\mathrm{t}}I_{-m-1}=0, \qquad m\ge M, \tag{2.3}$$

where for brevity we let $\mu_{\mathrm{t}}=\mu_{\mathrm{a}}+\mu_{\mathrm{s}}$. In particular, (2.3) shows that the sequence $\mathbf{I}=(I_{-m}|_\Omega\,;\,m\ge M)$ solves

$$\overline{\partial}\mathbf{I}+\mathcal{L}^2\partial\mathbf{I}+\mu_{\mathrm{t}}\mathcal{L}\mathbf{I}=0,\ \text{in }\Omega, \tag{2.4}$$

where $\mathcal{L}$ denotes the left shift operator $\mathcal{L}(I_{-M},I_{-M-1},\dots)=(I_{-M-1},I_{M-2},\dots)$ and $\mathcal{L}^2$ is the double shift.

One key fact in the reconstruction method is that solutions of (2.4) are in a one-to-one correspondence with solutions $\mathbf{J}=(J_{-m}|_\Omega\,;\,m\ge M)$ of the $\mathcal{L}^2$-analytic equation

$$\overline{\partial}\mathbf{J}+\mathcal{L}^2\partial\mathbf{J}=0\ \text{ in }\Omega. \tag{2.5}$$

This correspondence is via the convolution with the Fourier sequence of the special integrating factor originally introduced in [6]. More precisely, let

$$h[\mu_{\mathrm{t}}](z,\xi):=D[\mu_{\mathrm{t}}](z,\xi)-\frac{1}{2}(I-iH)R[\mu_{\mathrm{t}}](z\cdot\xi^\perp,\xi^\perp), \tag{2.6}$$

where $\xi^\perp$ is the counterclockwise rotation of ξ by $\pi/2$, D is the divergent beam transform

$$D[\mu_{\mathrm{t}}](z,\xi)=\int_0^\infty\mu_{\mathrm{t}}(z+t\xi)\,dt,$$

R is the Radon transform in $\mathbb{R}^2$,

$$R[\mu_{\mathrm{t}}](s,\xi)=\int_{\mathbb{R}}\mu_{\mathrm{t}}(s\xi+t\xi^\perp)\,dt,$$

and H is the Hilbert transform

$$H[f](s)=\frac{1}{\pi}\mathrm{p.v.}\int_{\mathbb{R}}\frac{f(t)}{s-t}\,dt.$$

As shown in [6], for each $z\in\Omega$, the map $\xi\mapsto h(z,\xi)$ is the trace on the circle of an analytic function in the unit disc. In particular, h and, thus $e^{\pm h}$ have only positive Fourier modes

$$e^{-h[\mu_{\mathrm{t}}](z,\xi(\theta))}=\sum_{m=0}^\infty\alpha_m(z)e^{im\theta},\quad (z,\xi)\in\overline{\Omega}\times S^1,$$

and

$$e^{+h[\mu_t](z,\xi(\theta))} = \sum_{m=0}^{\infty} \beta_m(z) e^{im\theta}, \quad (z,\xi) \in \overline{\Omega} \times S^1.$$

If we define

$$J_{-m}(z) = \sum_{j=0}^{\infty} \alpha_j(z) I_{-m-j}(z), \quad z \in \overline{\Omega}, m \geq 0, \tag{2.7}$$

then one uses the fact that $\xi \cdot \nabla h(z,\xi) = -\mu_t(z)$ to check that $\mathbf{J}$ solves the $\mathcal{L}^2$-analytic equation (2.5). Moreover, given $\mathbf{J}$, one recovers $\mathbf{I}$ via

$$I_{-m}(z) = \sum_{j=0}^{\infty} \beta_j(z) J_{-m-j}(z), \quad z \in \overline{\Omega}, \quad m \geq 0. \tag{2.8}$$

We refer to [27, 28] for details.

Solutions to (2.5) are said to be $\mathcal{L}^2$-analytic in the sense of Bukhgeim [3]. An important property of $\mathcal{L}^2$-analytic sequences is that they obey a Cauchy-like integral formula. For any simple piecewise-smooth closed curve $\gamma \subset \overline{\Omega}$, the values of $\mathbf{J}$ at any point enclosed by γ is determined by the values of $\mathbf{J}$ on γ. More precisely, for z enclosed by γ,

$$\begin{aligned} J_{-m}(z) = {} & \frac{1}{2\pi i} \int_\gamma \frac{J_{-m}(\zeta)}{\zeta - z} d\zeta \\ & + \frac{1}{2\pi i} \int_\gamma \left(\frac{d\zeta}{\zeta - z} - \frac{d\overline{\zeta}}{\overline{\zeta} - \overline{z}} \right) \left\{ \sum_{j=1}^{\infty} J_{-m-2j}(\zeta) \left(\frac{\overline{\zeta} - \overline{z}}{\zeta - z} \right)^j \right\} d\zeta, \quad m \geq M. \end{aligned} \tag{2.9}$$

If we were to measure the outflow I on the entire boundary $\partial\Omega$, then (2.7) would yield $(J_{-m}|_{\partial\Omega}\,;\, m \geq M)$ on the boundary, and (2.9) would give $(J_{-m}|_{\Omega}\,;\, m \geq M)$ in Ω, and then via (2.1) the source q would be obtained in Ω. This was the strategy used in [8, 9]. However, in our problem I is only known on the open arc Λ; see Figure 1.

Upon a rotation and translation of the domain, we may assume that the chord C joining the endpoints of Λ is the interval $(-c, c)$ on the real axis for some $c > 0$. We may also assume that Λ lies in the upper half plane $\{\mathrm{Im}(z) > 0\}$.

Using (2.9) on $\Lambda \cup C$ and taking the limit $\Omega^+ \ni z \to x \in C$, the second term in the right-hand side vanishes by virtue of continuity [28]. Hence the Sokhotski–Plemelj formula yields the CSIE

$$(I - iH_c) J_{-m}(x) = 2P^-[J_{-m}|_\Lambda](x), \quad x \in C, \tag{2.10}$$

where

$$\begin{aligned} P^-[J_{-m}|_\Lambda](z) = {} & \frac{i}{2\pi} \int_\Lambda \frac{J_{-m}(\zeta)}{z - \zeta} d\zeta \\ & - \frac{i}{2\pi} \int_\Lambda \left(\frac{d\zeta}{\zeta - z} - \frac{d\overline{\zeta}}{\overline{\zeta} - \overline{z}} \right) \sum_{j=1}^{\infty} J_{-m-2j}(\zeta) \left(\frac{\overline{\zeta} - \overline{z}}{\zeta - z} \right)^j, \quad z \in \overline{\Omega^+}, m \geq M. \end{aligned}$$

By solving (2.10), we determine the sequence $(J_{-m}|_C\,;\, m \geq M)$ on the chord C. Together with the data on Λ, the sequence $(J_{-m}|_{\partial\Omega^+}\,;\, m \geq M)$ is now known on $\partial\Omega^+$ and an application of (2.9) yields its values in Ω^+:

$$J_{-m}(z) = \frac{1}{2\pi i}\int_{-c}^{c} \frac{J_{-m}(t)}{t-z}dt + \frac{1}{2\pi i}\int_{-c}^{c}\left(\frac{1}{t-z}-\frac{1}{t-\overline{z}}\right)\left\{\sum_{j=1}^{\infty} J_{-m-2j}(t)\left(\frac{t-\overline{z}}{t-z}\right)^j\right\}dt + P^-[J_{-m}|_\Lambda](z), \quad z\in\Omega^+, m\geq M.$$

The system (2.2) yields a system of elliptic initial value problems for I_{-m}, $0 \leq m \leq M-1$, which can be solved iteratively in decreasing order of m starting with $m = M-1$, and ending with $m = 0$. More precisely, we obtain

$$\begin{cases} \overline{\partial} I_{-m} = f_{-m} & \text{in } \Omega^+,\ 0 \leq m \leq M-1; \\ I_{-m}|_\Lambda : \text{given}, \end{cases}$$

where $f_{-m} = -\partial I_{-m-2} + (2\pi\mu_{\mathrm{s}} p_{-m-1} - \mu_{\mathrm{t}}) I_{-m-1}$. The Cauchy–Pompeiu formula [34] yields

$$I_{-m}(z) = \frac{1}{2\pi i}\int_{\partial\Omega^+}\frac{I_{-m}(\zeta)}{\zeta - z}\,d\zeta - \frac{1}{\pi}\int_{\Omega^+}\frac{f_{-m}(\xi+i\eta)}{(\xi+i\eta)-z}\,d\xi\,d\eta. \tag{2.11}$$

Again, by taking the limit $\Omega^+ \ni z \to x \in C$ and using the Sokhotski–Plemelj formula, we obtain the CSIE

$$(I - iH_c)I_{-m}(x) = -\frac{2}{\pi}\int_{\Omega^+}\frac{f_{-m}(\xi+i\eta)\,d\xi\,d\eta}{(\xi-x)+i\eta} + \frac{1}{\pi i}\int_\Lambda \frac{I_{-m}(\zeta)}{\zeta - x}d\zeta, \quad x \in C. \tag{2.12}$$

This is again an equation like (2.10) with a different right-hand side. The solution to the equation (2.12) determines I_{-m} on the chord C.

Since the trace of $I_{-m}|_\Lambda$ on Λ is given for $0 \leq m \leq M$, we have now determined the trace of I_{-m} on the entire boundary of Ω^+. The values of I_{-m} in Ω^+ can be obtained by the Cauchy–Pompeiu formula (2.11):

$$I_{-m}(z) = -\frac{1}{\pi}\int_{\Omega^+}\frac{f_{-m}(\xi+i\eta)\,d\xi\,d\eta}{(\xi-z)+i\eta} + \frac{1}{2\pi i}\int_\Lambda\frac{I_{-m}(\zeta)}{\zeta-z}d\zeta + \frac{1}{2\pi i}\int_{-c}^{c}\frac{I_{-m}(x)}{x-z}\,dx.$$

With I_0 and I_{-1} now computed in Ω^+, the source q is determined via (2.1).

3. On the numerical stability in a singular integral equation of Cauchy type. A key step in our reconstruction procedure requires solving the Cauchy type singular integral equations (CSIE) (2.10) and (2.12), both of which are of the type

$$\phi(x) - \frac{i}{\pi}\mathrm{p.v.}\int_{-c}^{c}\frac{\phi(y)}{x-y}dy = \Phi(x), \quad x \in (-c,c). \tag{3.1}$$

Since the spectrum of iH_c with the finite Hilbert transform H_c in (1.4) is $[-1,1]$, the operator $[(1+\epsilon)I - iH_c]^{-1}$ is bounded on $L^2(-c,c)$ for any $\epsilon > 0$. This remark leads to the regularization of (3.1) via solutions to

$$(1+\epsilon)\phi_\epsilon(x) - \frac{i}{\pi}\text{p.v.}\int_{-c}^{c}\frac{\phi_\epsilon(y)}{x-y}dy = \Phi(x), \quad x \in (-c,c). \tag{3.2}$$

One could approach solving (3.2) by considering solutions to

$$(1+\epsilon)\phi_\epsilon(x) - \frac{b}{\pi}\text{p.v.}\int_{-c}^{c}\frac{\phi_\epsilon(y)}{x-y}dy = \Phi(x), \quad x \in (-c,c), \tag{3.3}$$

and then letting $b \to i$.

If b is a real number, it is well known [12, 24, 33] that, for any $\Phi \in L^2(-c,c)$ and $\epsilon > 0$, (3.3) has the unique solution given by

$$\phi_\epsilon(x) = \frac{(1+\epsilon)\Phi(x)}{(1+\epsilon)^2+b^2} - \frac{b}{\pi}\frac{e^{\tau(x)}}{(1+\epsilon)^2+b^2}\int_{-c}^{c}\frac{e^{-\tau(y)}\Phi(y)}{y-x}dy, \quad x \in (-c,c), \tag{3.4}$$

where

$$\tau(x) = -\frac{1}{\pi}\text{Arctan}\frac{b}{1+\epsilon}\log\frac{c-x}{c+x}.$$

The solution (3.4) depends continuously on the parameter b as long as $(1+\epsilon)^2+b^2 \neq 0$. For $\epsilon > 0$ fixed, since $(1+\epsilon)^2+b^2 \neq 0$ for b along the segment joining 0 and i, the solution to (3.2) is obtained by setting $b = i$ in (3.4). In the numerical evaluation we are then led to calculate

$$e^{\tau(x)} = \cos\left(\gamma\log\frac{c+x}{c-x}\right) + i\sin\left(\gamma\log\frac{c+x}{c-x}\right), \tag{3.5}$$

where

$$\gamma = \frac{1}{2\pi}\log\frac{2+\epsilon}{\epsilon}.$$

However, infinite oscillations near the end points $x = \pm c$ make the numerical treatment of e^τ difficult. While one could try some particular numerical integration scheme, e.g., as in [32], choosing optimal truncation parameters seems nontrivial.

It is also known [5] that the solution to (3.3) can be approximated by

$$\phi_\epsilon(x) \approx \sum_n C_n w(x/c) P_n^{(\mu,\nu)}(x/c),$$

where

$$\mu = -\nu = \frac{1}{2\pi i}\log\frac{2+\epsilon}{\epsilon}, \qquad w(t) = (1-t)^\mu(1+t)^\nu,$$

and $P_n^{(\mu,\nu)}(t)$ is the Jacobi polynomial. In this algorithm the coefficients C_n are given by

$$C_n = -\frac{1}{b}\frac{\sin\pi\mu}{\theta_n^{(\mu,\nu)}}\int_{-1}^{1} P_n^{(-\mu,-\nu)}(t)w^{-1}(t)\Phi(ct)\,dt,$$

with

$$\theta_n^{(\mu,\nu)} = \frac{2^{\mu+\nu+1}}{2n+\mu+\nu+1}\frac{\Gamma(n+\mu+1)\Gamma(n+\nu+1)}{n!\,\Gamma(n+\mu+\nu+1)}.$$

Unfortunately, due to the presence of the factor $1/w$ in the integrand, the numerical integration in C_n is as inefficient as using the solution formula (3.5).

To circumvent these inefficiencies we propose solving (3.2) via a Galerkin approximation scheme.

Let N be a positive integer, let $I_m = (-c+(m-1)\Delta x, -c+m\Delta x)$ denote equi-spaced intervals on $(-c,c)$ with $\Delta x = 2c/N$, and let x_m be the midpoint of I_m. Let $\chi_m(x)$ be the characteristic of I_m. The approximation

$$\phi_{\epsilon,\Delta} = \sum_{k=1}^{N}\phi_{\epsilon,k}\chi_k(x)$$

to ϕ_ϵ in $L^2(-c,c)$ by elements in $\operatorname{span}\{\chi_m\,;\,1\le m\le N\}$ reduces (3.2) to the semidiscrete equation

$$(1+\epsilon)\phi_{\epsilon,m}\Delta x - \frac{i}{\pi}\sum_{k=1}^{N}\phi_{\epsilon,k}\int_{-c}^{c}\left(\text{p.v.}\int_{-c}^{c}\frac{\chi_k(y)\,dy}{x-y}\right)\chi_m(x)\,dx \approx \int_{-c}^{c}\Phi(x)\chi_m(x)\,dx, \quad 1\le m\le N. \tag{3.6}$$

Furthermore, by adopting the midpoint rule,

$$\begin{aligned}\int_{-c}^{c}\left(\text{p.v.}\int_{-c}^{c}\frac{\chi_k(y)\,dy}{x-y}\right)\chi_m(x)\,dx &\approx \text{p.v.}\int_{-c}^{c}\frac{\chi_k(y)\,dy}{x_m-y}\Delta x\\ &\approx \left(\int_{-c}^{x_m-\Delta x/2}+\int_{x_m+\Delta x/2}^{c}\right)\frac{\chi_k(y)\,dy}{x_m-y}\Delta x\\ &= \begin{cases}0, & k=m;\\ \Delta x\displaystyle\int_{I_k}\frac{dy}{x_m-y}\approx\frac{\Delta x^2}{x_m-x_k}, & k\ne m,\end{cases}\end{aligned}$$

(3.6) reduces to the linear system

$$(1+\epsilon)\phi_{\epsilon,m} - \frac{i}{\pi}\sum_{k\ne m}\frac{\phi_{\epsilon,k}}{m-k} = \Phi_m, \quad 1\le m\le N, \tag{3.7}$$

where

$$\Phi_m = \frac{1}{\Delta x}\int_{I_m}\Phi(x)\,dx \quad\text{or}\quad \Phi(x_m).$$

Note that (3.7) could also be interpreted as the discretization by the collocation method and the composite midpoint rule, where $\phi_{\epsilon,m}$ would correspond to $\phi_\epsilon(x_m)$.

Let H_N be a square matrix of order N whose (m,k)-entry is

$$h_{mk} = \begin{cases} \frac{1}{\pi}\frac{1}{m-k}, & m \neq k; \\ 0, & m = k. \end{cases}$$

The norm of H_N in ℓ^2 norm as a linear transformation on $\mathbb{C}^N$ is known from Montgomery–Matthews' inequality [17, 22, 23] to be estimated by

$$\|H_N\|_2 \leq 1 - \frac{1}{N}. \tag{3.8}$$

As a direct corollary, our proposed numerical procedure satisfies the following properties.

Theorem 3.1. *For any $\epsilon \geq 0$ and any positive integer N, $(1+\epsilon)E_N - iH_N$ is strictly positive definite on $\mathbb{C}^N$, where E_N is the identity matrix of order N. Moreover, the condition number in the 2-norm is estimated by the following:*

- *if $\epsilon = 0$, then*

$$\mathrm{cond}_2(E_N - iH_N) \leq 2N - 1, \tag{3.9}$$

  and it grows at most linearly with respect to N;
- *if $\epsilon > 0$, then*

$$\mathrm{cond}_2\Big[(1+\epsilon)E_N - iH_N\Big] \leq 1 + \frac{2}{\epsilon} \tag{3.10}$$

  is uniformly bounded with respect to N.

Proof. Noting that $(1+\epsilon)E_N - iH_N$ is Hermitian, suppose that $\lambda \in \mathbb{R}$ satisfies $[(1+\epsilon)E_N - iH_N]x = \lambda x$ with some $x \in \mathbb{C}^N \setminus \{0\}$. Then, $iH_N x = (1+\epsilon-\lambda)x$ and by the Montgomery–Matthews' inequality (3.8),

$$|1+\epsilon-\lambda| \leq \|H_N\|_2 \leq 1 - \frac{1}{N}.$$

Therefore

$$0 < \epsilon + \frac{1}{N} \leq \lambda \leq 2 + \epsilon - \frac{1}{N}.$$

■

Theorem 3.2. *For any $\epsilon \geq 0$, positive integer N, and $(\Phi_m) \in \mathbb{C}^N$, there exists a unique solution $(\phi_{\epsilon,m}) \in \mathbb{C}^N$ to (3.7).*

Theorem 3.2 directly guarantees that the algorithm proposed in the next section does not break down.

One may derive more accurate discretization to solve (3.2) by choosing proper collocation points [5] that adapt to the singularity of the solution at the end points, or more accurate

quadrature methods. For example, if $\phi \in C^2$ in a neighborhood of the chord C, then the principal value integral can be evaluated as in [9, 19], and then (3.2) becomes

$$(1+\epsilon)\phi_\epsilon(x) - \frac{i}{\pi}\left(-\int_{-c}^{c}\psi(x,y)\,dy + \phi_\epsilon(x)\log\frac{c+x}{c-x}\right) = \Phi(x),$$

with

$$\psi(x,y) = \begin{cases} \dfrac{\phi_\epsilon(x)-\phi_\epsilon(y)}{x-y}, & x \neq y; \\ \phi_\epsilon'(x), & x = y. \end{cases}$$

Note that the integral on the left-hand side is now in the sense of Riemann. The composite midpoint rule and second-order approximations to ϕ_ϵ' yields the linear system

$$\left(1+\epsilon - \frac{i}{\pi}\log\frac{c+x_m}{c-x_m} + \frac{i}{\pi}\sum_{k\neq m}\frac{1}{m-k}\right)\phi_{\epsilon,m} - \frac{i}{\pi}\sum_{k\neq m}\frac{\phi_{\epsilon,k}}{m-k} + \frac{i}{\pi}\begin{Bmatrix} -\frac{1}{2}\phi_{\epsilon,3} + 2\phi_{\epsilon,2} - \frac{3}{2}\phi_{\epsilon,1}, & m=1, \\ \frac{1}{2}\phi_{\epsilon,m+1} - \frac{1}{2}\phi_{\epsilon,m-1}, & 1<m<N, \\ \frac{1}{2}\phi_{\epsilon,N-2} - 2\phi_{\epsilon,N-1} + \frac{3}{2}\phi_{\epsilon,N}, & m=N \end{Bmatrix} = \Phi_m, \quad 1 \le m \le N. \tag{3.11}$$

To differentiate between the numerical method that uses (3.7) from the one that uses (3.11) in the numerical solvability of the singular integral equation (3.2), we call the former the *cut-off method*, and the latter the *extracting logarithmic singularity (ex-log) method*.

The condition numbers of (3.7) and (3.11) for $\epsilon = 0$, 0.01, and 0.1 obtained numerically are depicted in Figure 2 where the horizontal axis is the size of the matrix N and the vertical axis is the condition number in the logarithmic scale. These results indicate that (3.7) is numerically more stable than (3.11), and the instability of (3.7) with $\epsilon = 0$ is not serious.

4. Reconstruction algorithm.

In this section, we present the numerical algorithm for the source reconstruction.

Recall that the absorbing and scattering medium (as characterized by μ_a, μ_s in Ω, and p in Ω^+) is known. Assume that Λ has a smooth parameterization $\zeta(\omega)$ for $\omega^- \le \omega \le \omega^+$, with $\zeta(\omega^\mp) = \pm c$. Outflow through Λ, $I_{\text{measured}}(\zeta,\xi)$, is sampled at $(\zeta_k, \xi(\theta_t)) \in \Gamma_+$ with $\zeta_k \in \Lambda$, where $\zeta_1, \ldots, \zeta_K$ are K distinct points on Λ, and $\theta_t = 2\pi t/T$ for a positive integer T. We assume that $\zeta_k = \zeta(\tilde\omega_k)$ and $\omega^- < \tilde\omega_1 < \tilde\omega_2 < \cdots < \tilde\omega_K < \omega^+$.

Step 1. Let $\omega_k = (\tilde\omega_k + \tilde\omega_{k+1})/2$ for $1 \le k \le K-1$, $\omega_0 = \omega^-$, and $\omega_K = \omega^+$. Write $\Delta\omega_k = \omega_k - \omega_{k-1}$ and $\zeta_k' = \zeta'(\tilde\omega_k)$ for $1 \le k \le K$. This leads an approximation by the composite midpoint rule

$$\int_\Lambda f(\zeta)\,d\zeta \approx \sum_{k=1}^{K} f(\zeta_k)\zeta_k'\Delta\omega_k.$$

Step 2. We introduce an inscribed polygonal domain $\Omega_\Delta^+ \approx \Omega^+$ whose closure includes C and take a triangulation $\mathcal{T} = \{\tau_\ell\}$ of Ω_Δ^+, i.e., each τ_ℓ is a triangular domain, $\tau_\ell \cap \tau_k = \emptyset$ if

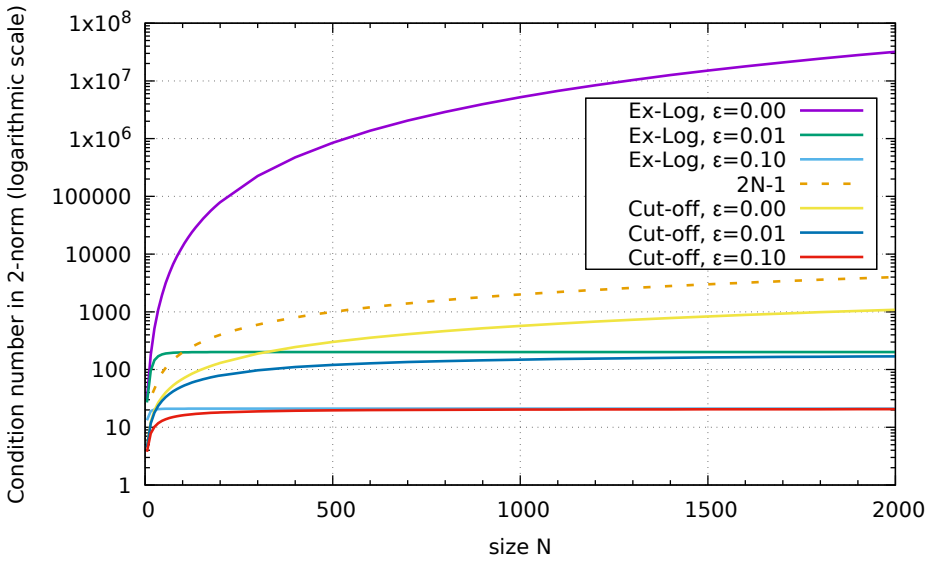

Figure 2. *Condition numbers in* 2*-norm to linear systems by the cut-off method* (3.7) *and the ex-log method* (3.11).

$\ell \neq k$, and $\overline{\Omega_\Delta^+} = \bigcup_\ell \overline{\tau_\ell}$. Let $P_1(\mathcal{T})$ denote the set of the piecewise linear continuous functions with respect to $\mathcal{T}$. We denote by V the set of vertices of $\mathcal{T}$, and by r_ℓ the centroid of τ_ℓ.

Step 3. Fix positive integers N, $\tilde{M}$, and S. On the chord C, we allocate nodes $x_n = -c + (n-1/2)\Delta x$, $1 \le n \le N$ with $\Delta x = 2c/N$. These are involved in the composite midpoint rule on C as

$$\int_C f(x)\,dx \approx \sum_{n=1}^{N} f(x_n)\Delta x.$$

The integer S should be chosen sufficiently large to truncate (2.3), at least $S \ge \tilde{M} + 3$.

Step 4. For $0 \le m \le S$ and $\zeta_k \in \Lambda$, compute

$$\alpha_{m,k} = \frac{1}{T}\sum_{t=0}^{T-1} \exp\Big(-h[\mu_t](\zeta_k, \xi(\theta_t))\Big) e^{-i(-m)\theta_t}.$$

Step 5. For $0 \le m \le S - \tilde{M} - 2$, compute

$$\beta_{m,\ell} = \frac{1}{T}\sum_{t=0}^{T-1} \exp\Big(h[\mu_t](z_\ell, \xi(\theta_t))\Big) e^{-i(-m)\theta_t}, \qquad z_\ell \in V$$

and

$$\beta_{m,n}^C = \frac{1}{T}\sum_{t=0}^{T-1} \exp\Big(h[\mu_t](x_n, \xi(\theta_t))\Big) e^{-i(-m)\theta_t}, \qquad x_n \in C.$$

The function $h[\mu_t]$ is evaluated by the use of midpoint rule with a quadrature rule taking the singularity of the Cauchy kernel into account [9, 19].

Step 6. For $0 \le m \le S$, compute

$$\mathcal{I}^{\Lambda}_{-m,k} = \frac{1}{T}\sum_{t=0}^{T-1} I_{\mathrm{bd}}(\zeta_k, \xi(\theta_t)) e^{i(-m)\theta_t}, \quad \zeta_k \in \Lambda,$$

where

$$I_{\mathrm{bd}}(\zeta_k, \xi(\theta_t)) = \begin{cases} I_{\mathrm{measured}}(\zeta_k, \xi(\theta_t)) & \text{on } \Gamma_+; \\ 0 & \text{on } \Gamma_-. \end{cases}$$

Let $\mathcal{I}^{\Lambda}_{-m}$ a piecewise constant approximation: $\mathcal{I}^{\Lambda}_{-m}(\zeta(\omega)) = \mathcal{I}^{\Lambda}_{-m,k}$, $\omega_{k-1} < \omega < \omega_k$.

Step 7. For $\tilde{M} \le m \le S$, compute

$$\mathcal{J}^{\Lambda}_{-m,k} = \sum_{s=0}^{S-m} \alpha_{s,k} \mathcal{I}^{\Lambda}_{-m-s,k}, \quad \zeta_k \in \Lambda.$$

Step 8. For $m = S-2, S-3, \ldots, \tilde{M}$, find the solution to the system of linear equations

$$(E_N - iH_N) \begin{pmatrix} \mathcal{J}^{C}_{-m,1} \\ \vdots \\ \mathcal{J}^{C}_{-m,N} \end{pmatrix} = \begin{pmatrix} \mathcal{P}^{-}_{-m}(x_1) \\ \vdots \\ \mathcal{P}^{-}_{-m}(x_N) \end{pmatrix},$$

where

$$\mathcal{P}^{-}_{-m}(x) = \frac{i}{2\pi}\sum_{k=1}^{K} \frac{\zeta_k' \Delta\omega_k}{x - \zeta_k} \mathcal{J}^{\Lambda}_{-m,k} + \frac{1}{\pi}\sum_{k=1}^{K} \left\{ \mathrm{Im}\left(\frac{\zeta_k'}{\zeta_k - x}\right) \Delta\omega_k \right\} \left\{ \sum_{m+2 \le m+2j \le S} \mathcal{J}^{\Lambda}_{-m-2j,k} \left(\frac{\overline{\zeta_k} - \overline{x}}{\zeta_k - x}\right)^j \right\}.$$

Step 9. Compute $\mathcal{J}^{\Omega^+}_{-m}(z_\ell)$ for $\tilde{M} \le m \le S-2$ and $z_\ell \in V \cap \Omega^+$, where

$$\mathcal{J}^{\Omega^+}_{-m}(z) = \mathcal{P}^{-}_{-m}(z) + \frac{\Delta x}{2\pi i}\sum_{n=1}^{N} \frac{1}{x_n - z} \mathcal{J}^{C}_{-m,n} + \frac{\Delta x}{2\pi i}\sum_{n=1}^{N} \left(\frac{1}{x_n - z} - \frac{1}{x_n - \overline{z}}\right) \left\{ \sum_{m+2 \le m+2j \le S} \mathcal{J}^{C}_{-m-2j,n} \left(\frac{x_n - \overline{z}}{x_n - z}\right)^j \right\}.$$

Step 10. For $z_\ell \in V \cap \Omega^+$, compute

$$\mathcal{I}^{\Omega^+}_{-\tilde{M},\ell} = \sum_{s=0}^{S-\tilde{M}-2} \beta_{s,\ell} \mathcal{J}^{\Omega^+}_{-\tilde{M}-s}(z_\ell)$$

and

$$\mathcal{I}^{\Omega^+}_{-\tilde{M}-1,\ell} = \sum_{s=0}^{S-\tilde{M}-3} \beta_{s,\ell} \mathcal{J}^{\Omega^+}_{-\tilde{M}-1-s}(z_\ell).$$

Step 11. For $x_n \in C$, compute

$$\mathcal{I}^{C}_{-\tilde{M},n} = \sum_{s=0}^{S-\tilde{M}-2} \beta^{C}_{s,n} \mathcal{J}^{C}_{-\tilde{M}-s,n}$$

and

$$\mathcal{I}^{C}_{-\tilde{M}-1,n} = \sum_{s=0}^{S-\tilde{M}-3} \beta^{C}_{s,n} \mathcal{J}^{C}_{-\tilde{M}-1-s,n}.$$

For $m = \tilde{M}, \tilde{M}+1$, denote by $\mathcal{I}^{C}_{-m}$ the piecewise constant approximation on C: $\mathcal{I}^{C}_{-m}(x) = \sum_{n=1}^{N} \mathcal{I}^{C}_{-m} \chi_n(x)$.

Step 12. Find $\mathcal{I}^{\partial\Omega^+}_{-\tilde{M}} = \sum a_j \varphi_j \in P_1(\partial\Omega^+_\Delta)$ by the L^2-best approximation to $\mathcal{I}^{\Lambda}_{-\tilde{M}}$ (of Step 6) and $\mathcal{I}^{C}_{-\tilde{M}}$ (of Step 11), where φ_j is the periodic and piecewise linear continuous function on $\partial\Omega^+$ with $\varphi_j(v_k) = \delta_{jk}$ (Kronecker's delta) and $v_k \in V \cap \partial\Omega^+$. For a more detailed example, see [9]. Now, $\{\mathcal{I}^{\Omega^+}_{-\tilde{M},\ell}; z_\ell \in V \cap \Omega^+\}$ in Step 10 and $\mathcal{I}^{\partial\Omega^+}_{-\tilde{M}}$ uniquely determine $\mathcal{I}_{-\tilde{M}} \in P_1(\mathcal{T})$.

Similarly, we can obtain $\mathcal{I}_{-\tilde{M}-1} \in P_1(\mathcal{T})$.

Step 13. For $m = \tilde{M}-1, \tilde{M}-2, \ldots, 1, 0$ (in descending order), find $\mathcal{I}_m \in P_1(\mathcal{T})$ as follows. Assume that $\mathcal{I}_{-m-2}, \mathcal{I}_{-m-1} \in P_1(\mathcal{T})$ are already computed. If $\mathcal{I}_{-m-2}|_{\tau_\ell} = a_\ell x_1 + b_\ell x_2 + c_\ell$, then $\partial\mathcal{I}_{-m-2}|_{\tau_\ell} = (a_\ell - i b_\ell)/2$. For $\tau_\ell \in \mathcal{T}$ compute

$$\mathcal{F}_{-m,\ell} = -\partial\mathcal{I}_{-m-2}|_{\tau_\ell} + \{2\pi\mu_{\mathrm{s}}(r_\ell) p_{-m-1}(r_\ell) - \mu_{\mathrm{t}}(r_\ell)\}\mathcal{I}_{-m-1}(r_\ell).$$

Compute for $x_n \in C$,

$$\mathcal{R}_{-m,n} = -\frac{2}{\pi} \sum_{\tau_\ell \in \mathcal{T}} \frac{\mathcal{F}_{-m,\ell}|\tau_\ell|}{r_\ell - x_n} + \frac{1}{\pi i} \sum_{k=1}^{K} \frac{\zeta_k' \Delta\omega_k}{\zeta_k - x_n} \mathcal{I}^{\Lambda}_{-m,k},$$

where $|\tau_\ell|$ is the area of τ_ℓ, and r_ℓ is the complex representation of its coordinate. Then solve the linear equation

$$(E_N - iH_N) \begin{pmatrix} \mathcal{I}^{C}_{-m,1} \\ \vdots \\ \mathcal{I}^{C}_{-m,N} \end{pmatrix} = \begin{pmatrix} \mathcal{R}_{-m,1} \\ \vdots \\ \mathcal{R}_{-m,N} \end{pmatrix}.$$

And compute for $z_\ell \in V \cap \Omega^+$,

$$\mathcal{I}^{\Omega^+}_{-m,\ell} = -\frac{1}{\pi} \sum_{\tau_j \in \mathcal{T}} \frac{\mathcal{F}_{-m,j}|\tau_j|}{r_j - z_\ell} + \frac{1}{2\pi i} \sum_{k=1}^{K} \frac{\zeta_k' \Delta\omega_k}{\zeta_k - z_\ell} \mathcal{I}^{\Lambda}_{-m,k} + \frac{\Delta x}{2\pi i} \sum_{n=1}^{N} \frac{\mathcal{I}^{C}_{-m,n}}{x_n - z_\ell},$$

with r_j expressed in $\mathbb{C}$ again. For $z_\ell \in V \cap \partial\Omega^+$, find $\mathcal{I}_{-m}^{\partial\Omega^+} \in P_1(\partial\Omega_\Delta^+)$ by the best approximation in the L^2 sense to $\mathcal{I}_{-m}^{\Lambda}$ and $\mathcal{I}_{-m}^{C}$ similarly to Step 12.

These $\{\mathcal{I}_{-m,\ell}^{\Omega^+}\,;\, z_\ell \in V \cap \Omega^+\}$ and $\mathcal{I}_{-m}^{\partial\Omega^+}$ give $\mathcal{I}_{-m} \in P_1(\mathcal{T})$.

Step 14. For each triangle $\tau_\ell \in \mathcal{T}$, let $\mathcal{I}_{-1}|_{\tau_\ell} = a_\ell x_1 + b_\ell x_2 + c_\ell$. The reconstruction of $q|_{\tau_\ell}$ is given by (2.1),

$$q_\ell = \mathrm{Re}(a_\ell) + \mathrm{Im}(b_\ell) + \{\mu_{\mathrm{t}}(r_\ell) - 2\pi\mu_{\mathrm{s}}(r_\ell)p_0(r_\ell)\}\mathrm{Re}(\mathcal{I}_0(r_\ell)).$$

This ends the algorithm.

We remark here on the dual role played by the truncation parameter $\tilde{M}$ as a regularization parameter to control both accuracy and stability. On the one hand $\tilde{M}$ sets the degree of the trig-polynomial (in the angular variable) approximation of the scattering phase function $p(z;\cdot)$ influencing the accuracy. On the other hand, the terms after the $\tilde{M}$th mode in the system (2.2) are truncated, thus resulting in (2.3). This also leads to truncation of higher frequency modes of the solution, which, in general, help the stabilization of the numerical procedure. Since the present algorithm gives a pointwise reconstruction, one may choose a locally optimal $\tilde{M}$, e.g., by observing (for several values of $\tilde{M}$) the degradation of accuracy in integration due to the singularities of the Cauchy kernel near the boundary.

5. Numerical experiments. In this section the proposed algorithm is demonstrated to show its validity. In particular, numerical results by the cut-off method (3.7) and the ex-log method (3.11) are compared to solve CSIEs. An example of choice of parameters are also exhibited. Throughout this section, all computations are processed on EPYC 7643 with the IEEE754 double precision arithmetic.

Revisiting the example in [10], suppose that Ω is the unit disk with inclusions

$$B_1 = \{(z_1, z_2)\,;\, (z_1 - 0.5)^2 + z_2^2 < 0.3^2\},$$
$$B_2 = \left\{(z_1, z_2)\,;\, (z_1 + 0.25)^2 + \left(z_2 - \frac{\sqrt{3}}{4}\right)^2 < 0.2^2\right\},$$
$$B_3 = \{(z_1, z_2)\,;\, z_1^2 + (z_2 + 0.6)^2 < 0.3^2\},$$

and

$$R = \{(z_1, z_2)\,;\, -0.25 < z_1 < 0.5, |z_2| < 0.15\}.$$

See Figure 3. The internal source q (to be recovered in Ω^+ in our inverse problem) is given by

$$q(z) = \begin{cases} 2 & \text{in } R; \\ 1 & \text{in } B_2 \cup B_3; \\ 0 & \text{otherwise.} \end{cases}$$

The attenuation coefficient $\mu_{\mathrm{t}} = \mu_{\mathrm{a}} + \mu_{\mathrm{s}}$ accounts for the absorption (via μ_{a}) and for the scattering off of the direction of counting (via μ_{s}). In our numerical experiment $\mu_{\mathrm{s}} = 3$ in Ω and

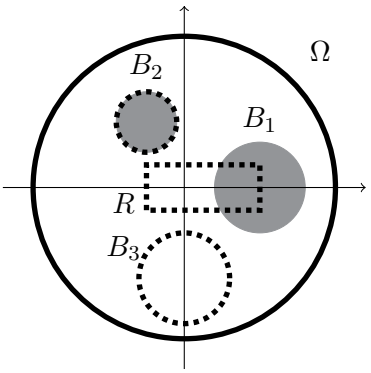

Figure 3. *An absorbing and scattering domain Ω: highly absorbing areas are B_1 and B_2; the internal source is supported in $B_2 \cup B_3 \cup R$.*

$$\mu_{\mathrm{a}}(z) = \begin{cases} 2 & \text{in } B_1; \\ 1 & \text{in } B_2; \\ 0.1 & \text{otherwise.} \end{cases}$$

The scattering kernel is the two-dimensional Henyey–Greenstein (Poisson) kernel

$$p(z; \xi \cdot \xi') = \frac{1}{2\pi} \frac{1 - g^2}{1 - (\xi \cdot \xi')g + g^2},$$

with $g = 0.5$.

Measurement data on the boundary arc Λ is obtained by the numerical computation of the forward problems (1.1) and (1.2) with the above choice of coefficients. We use the discontinuous Galerkin method with piecewise constant basis [7], where Ω and $S^1 \approx \mathbb{R}/2\pi$ are respectively divided into 27,407,104 triangular domains and 360 intervals with equal length. The outflow is measured at 3,141 equi-spaced nodes $\zeta \in \Lambda$ in direction $\xi \in S^1$ at 1 radian intervals with $(\zeta, \xi) \in \Lambda_+$. Figure 4 illustrates the computed outflow through a few points on the boundary arc Λ, where dependency on ξ is represented in the polar coordinate with the center ζ indicated by cross symbols ($\times$) and radius $2I(\zeta, \xi)$.

In the reconstruction, Step 2, the domain of interest Ω^+ is approximated by Ω^+_Δ and consists of 8,631 triangles. The number of triangles used in the reconstruction is much smaller than the one used in solving the forward problem, and they are not a sup-partition. In particular, the numerical experiments avoid an inverse crime.

In order to determine the truncation parameter S in Step 3, the decay of α_m and β_m are examined. Figure 5 presents $\max\{|\alpha_{m,k}| \,;\, \zeta_k \in \Lambda\}$ and $\max\{|\beta_{m,\ell}| \,;\, r_\ell \in \Omega^+\}$, where the horizontal axis is the mode m. The Hilbert transform is computed by the method in [9, 19] with the composite midpoint rule. A comparison of two discretizations is shown in Figure 5: The coarse discretization (indicated by the green + symbols) uses 100 spatial nodes for the Hilbert transform and 360 angles for the Fourier series, whereas the fine discretization (shown in purple $\times$ symbols) uses 10,000 spatial nodes and 2,880 angles. Both discretizations yield numerical results in good agreement with each other, and $\|\alpha_m\| < 0.01$ and $\|\beta_m\| < 0.01$ for

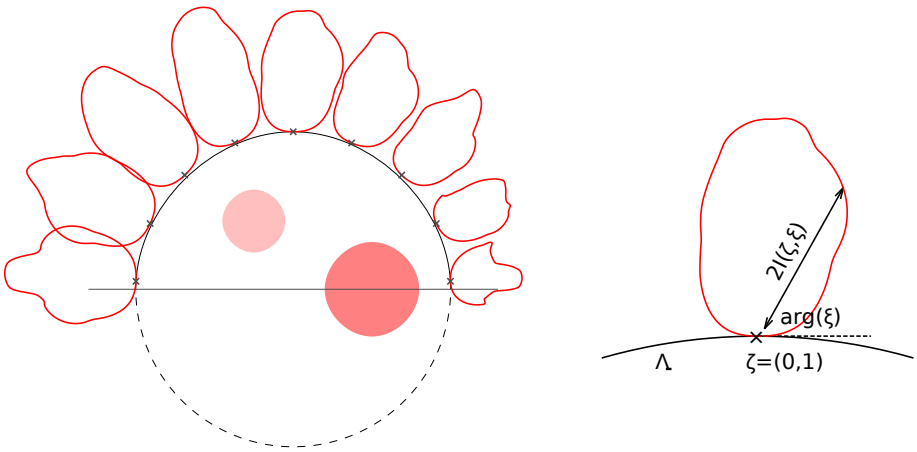

Figure 4. *Measurement data $I|_{\Lambda_+}$. The red curves depict the outflow $I(\zeta,\xi)$ in polar coordinate centered at ζ (cross symbol $\times$) and radius $2I(\zeta,\xi)$. The outflow through $\zeta=(0,1)$ is magnified in the right figure. The red inclusions show the highly absorbing regions given as a priori information (the medium is assumed to be known).*

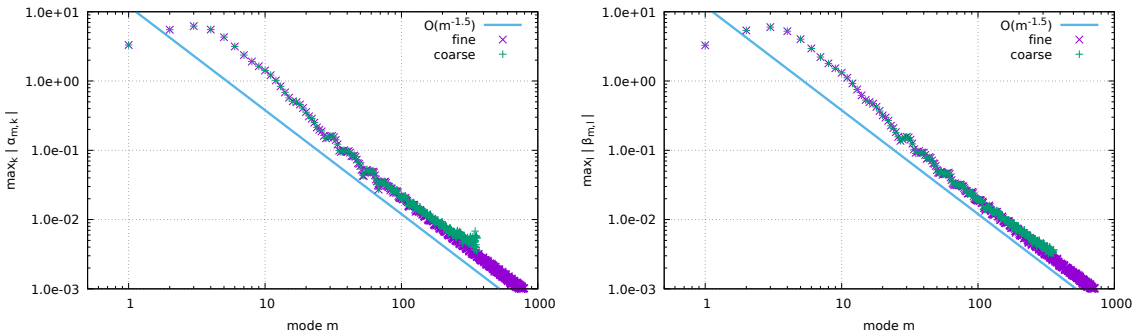

Figure 5. *Decay of $\|\alpha_m\|$ (left) and $\|\beta_m\|$ (right). Green plus (+) symbols are results by coarse discretization, while purple cross ($\times$) are those by fine discretization.*

$m \geq 175$. By taking the number of measured directions into account, we adopt $S = 175$ and use the coarse discretization.

To choose an optimal truncation parameter $\tilde{M}$ we use the criterion proposed in [9]. Namely, we compute the L^2-norms of the imaginary part of the reconstructed q for varying values of $\tilde{M}$, and choose the one corresponding to the smallest norm; see Figure 6. Note that in choosing $\tilde{M}$ we do not use information of the solution to the forward problem. For the estimate of error introduced by the truncation of the scattering kernel, we refer to [9] (Proposition 3.2). When the cut-off method with $\epsilon = 0$ is used, then $\|\mathrm{Im} q\|_2$ attains the minimum for $\tilde{M} = 10$, while $\tilde{M} = 12$ gives the minimum for the ex-log method with $\epsilon = 0.01$.

Note that the parameters $\tilde{M}$ and S are optimized without the use of the solution to the forward problem.

CSIEs in Steps 8 and 13 share the same coefficient matrix $(1+\epsilon)E_N - iH_N$, and thus it enables us to use LU decomposition for saving computational time. We take $N = 2{,}000$ so

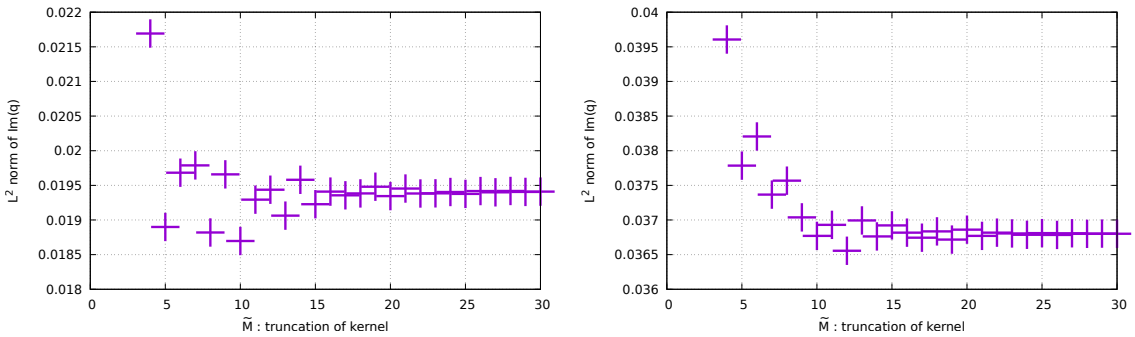

Figure 6. *$\|Imq\|_2$ of numerically reconstructed source. (Left) CSIEs are solved by the cut-off method with $\epsilon = 0$ yielding an optimal parameter $\tilde{M} = 10$. (Right) CSIEs are solved by the ex-log method with $\epsilon = 0.01$ yielding an optimal parameter $\tilde{M} = 12$.*

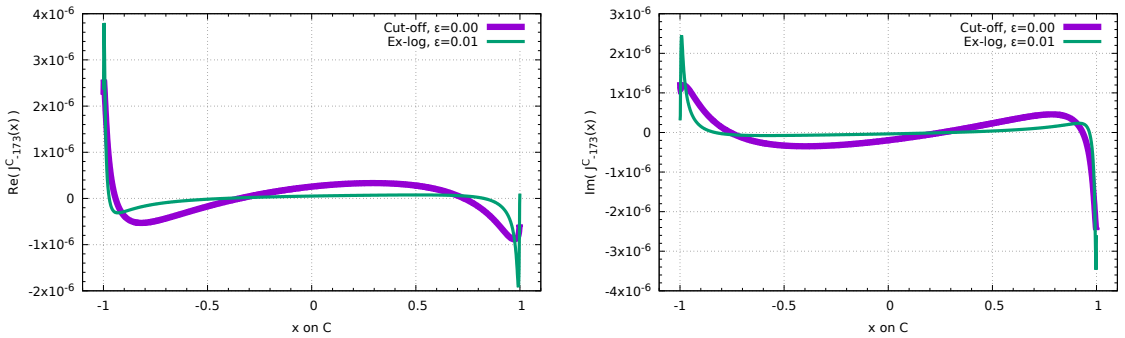

Figure 7. *Numerical solutions to CSIE, $\mathcal{J}^C_{-173,n}$ in Step 8. The left and right figures, respectively, show their real and imaginary parts.*

that $\Delta x = 0.001$ is close to $\Delta\omega = \pi/3{,}141$. Figure 7 depicts numerical solutions $\mathcal{J}^C_{-173,n}$ by the cut-off method with $\epsilon = 0$ and by the ex-log method with $\epsilon = 0.01$ as the first iteration, and they show similar trends. The results using the ex-log method with $\epsilon = 0$ are illustrated in Figure 8. Note that both the real and imaginary parts in Figure 8 oscillate in seriously wider vertical ranges than those in Figure 7. It shows that the ex-log method with $\epsilon = 0$ is worse ill-conditioned and harder to solve accurately. Numerical solutions $\mathcal{I}^C_{-1,n}$ and $\mathcal{I}^C_{0,n}$ as the final iterations in Step 13 are shown in Figure 9, and contrasted with those (in orange) computed directly using the numerical solution of the forward problem. Their real parts are similar characteristics, and relative magnitudes of their imaginary parts to real parts are also equivalently small. Figures 7 and 9 also indicate that numerical solutions by the ex-log method have sharp peaks near the edges, while the cut-off method generates milder variation.

In the cut-off method, the computation of $\mathcal{P}^-_{-m}$ in Step 8 took 233 seconds, while that of $\mathcal{J}^{\Omega^+}_{-m}$ in Step 9 took 1,093 seconds. These computations consume the bulk of the total computing time (of 1,393 seconds). However, due to the pointwise nature of the reconstruction, the proposed algorithm is amenable to parallelization. By using 48 threads of the OpenMP

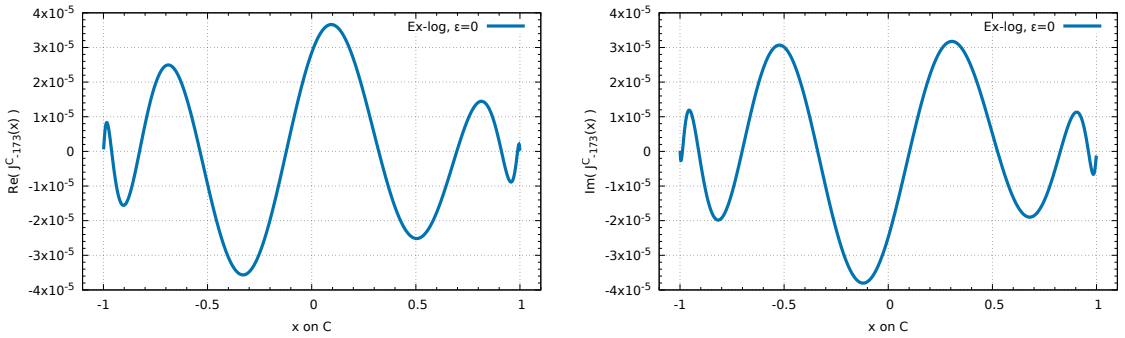

Figure 8. *The real (left) and imaginary (right) part of the numerical solutions to CSIE, $\mathcal{J}^C_{-173,n}$ in Step 8 by the ex-log method with $\epsilon = 0$.*

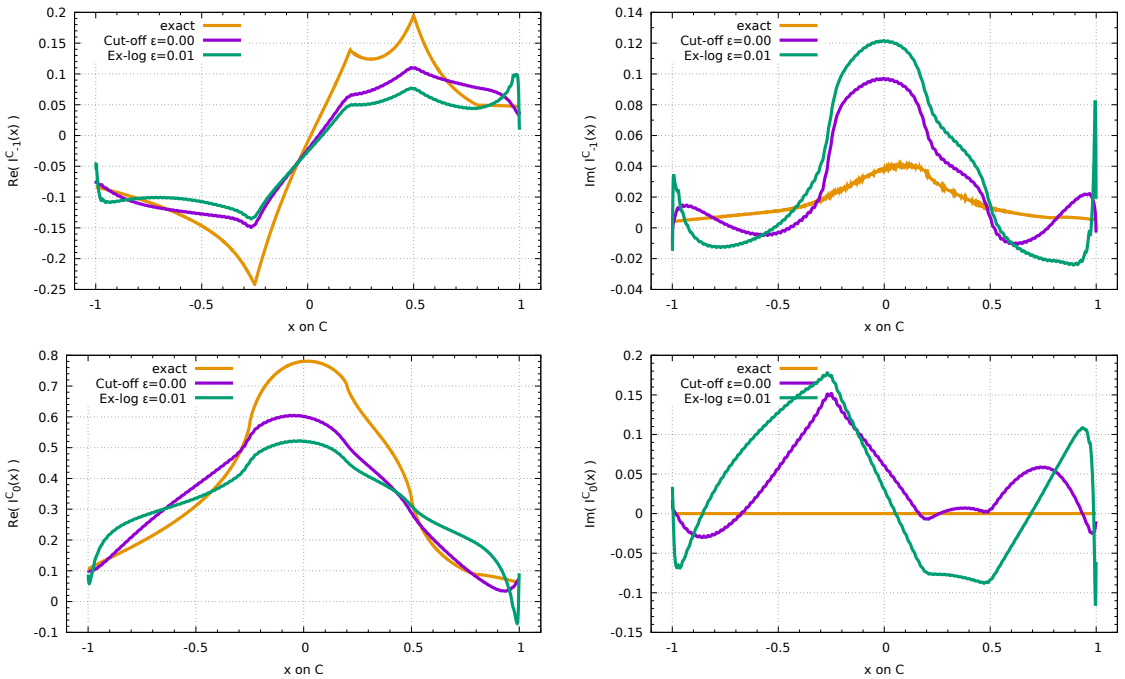

Figure 9. *Numerical solutions to CSIE, $\mathcal{I}^C_{-1,n}$ (upper) and $\mathcal{I}^C_{0,n}$ (lower) in Step 13. The left and right figures, respectively, show the real and imaginary parts.*

parallel computation, the total times for computing $\mathcal{P}^-_{-m}$ in Step 8 and $\mathcal{J}^{\Omega^+}_{-m}$ in Step 9 are reduced to 11 and 39 seconds, respectively, and the total time to 62 seconds. The numerically reconstructed source q in Ω^+ by the cut-off method with $\epsilon = 0$ is shown in Figure 10, and by the ex-log method with $\epsilon = 0.01$ is shown in Figure 11. The corresponding sections on the dotted line are shown in the same figure on the right. We note that the singular support of the internal sources is clearly identified, while the reconstructed values are quantitatively reasonable.

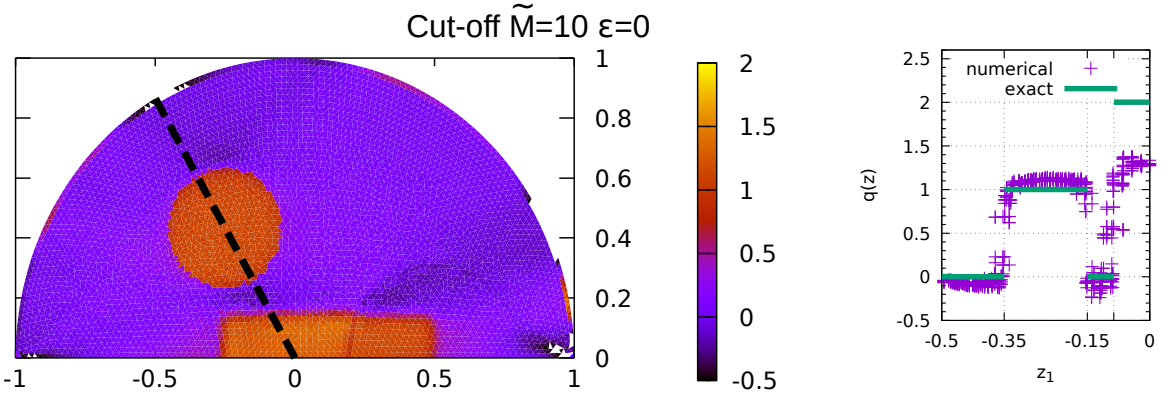

Figure 10. *Numerical reconstruction of the source q by the cut-off method in (3.7) without ϵ-regularization. On the right is the reconstructed section on the dotted segment.*

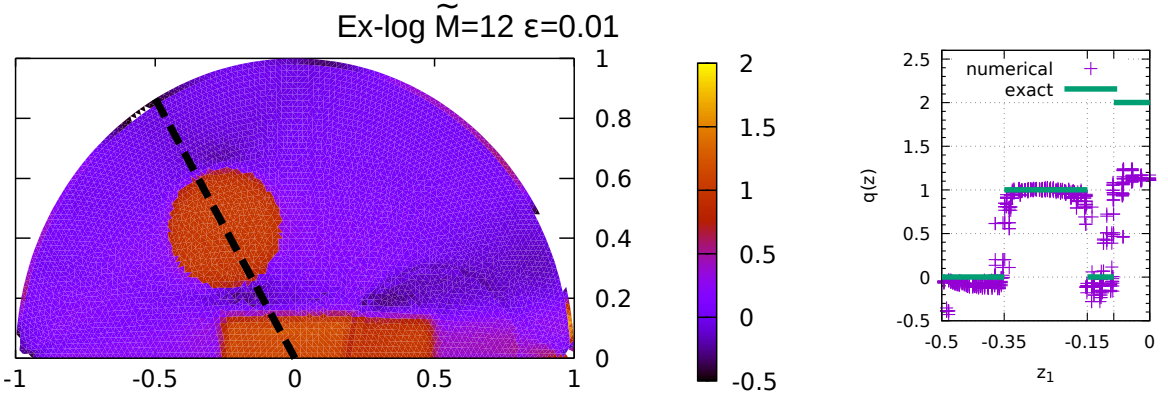

Figure 11. *Numerical reconstruction of the source q by (3.11) with $\epsilon = 0.01$. The right graph is its section on the dotted segment.*

Acknowledgment. The authors wish to thank Professor Keith Matthews for fruitful comments on the backgrounds of the Montgomery–Matthews' inequality.

REFERENCES

[1] F. Asllanaj, A. Addoum, and J. R. Roche, *Fluorescence molecular imaging based on the adjoint radiative transport equation*, Inverse Problems, 34 (2018), 075009.

[2] G. Bal and A. Tamasan, *Inverse source problems in transport equations*, SIAM J. Math. Anal., 39 (2007), pp. 57–76, https://doi.org/10.1137/050647177.

[3] A. L. Bukhgeim, *Inversion formulas in inverse problems*, in Linear Operators and Ill-Posed Problems, M. Lavrentiev and L. Ya. Savalev, eds., Plenum, New York, 1995, pp. 323–378.

[4] H. Egger and M. Schlottbom, *An L^p theory for stationary radiative transfer*, Appl. Anal., 93 (2014), pp. 1283–1296.

[5] F. Erdogan, G. D. Gupta, and T. S. Cook, *Numerical solution of singular integral equations*, in Mechanics of Fracture, Vol. 1, (1973), pp. 368–425.

[6] D. V. Finch, *The attenuated x-ray transform: Recent developments*, in Inside Out: Inverse Problems and Applications, Math. Sci. Res. Inst. Publ. 47, Cambridge University Press, Cambridge, 2003, pp. 47–66.

[7] H. Fujiwara, *Piecewise Constant Upwind Approximations to the Stationary Radiative Transport Equation*, Mathematics for Industry 34, Springer, Singapore, 2020, pp. 35–45.
[8] H. Fujiwara, K. Sadiq, and A. Tamasan, *A Fourier approach to the inverse source problem in an absorbing and anisotropic scattering medium*, Inverse Probl., 36 (2020), 015005.
[9] H. Fujiwara, K. Sadiq, and A. Tamasan, *Numerical reconstruction of radiative sources in an absorbing and nondiffusing scattering medium in two dimensions*, SIAM J. Imaging Sci., 13 (2020), pp. 535–555, https://doi.org/10.1137/19M1282921.
[10] H. Fujiwara, K. Sadiq, and A. Tamasan, *A source reconstruction method in two dimensional radiative transport using boundary data measured on an arc*, Inverse Problems, 37 (2021), 115005.
[11] H. Fujiwara, K. Sadiq, and A. Tamasan, *Partial inversion of the 2D attenuated X-ray transform with data on an arc*, Inverse Probl. Imaging, 16 (2022), pp. 215–228.
[12] F. D. Gakhov, *Boundary Value Problems*, Pergamon Press, Oxford, New York, Paris; Addison-Wesley, Reading, MA, London, 1966.
[13] M. A. Golberg, *Introduction to the numerical solution of Cauchy singular integral equations*, in Numerical Solution of Integral Equations, Math. Concepts Methods Sci. Engrg. 42, Plenum, New York, 1990, pp. 183–308.
[14] A. Hasanov and V. G. Romanov, *Introduction to Inverse Problems for Differential Equations*, Springer, Cham, 2017.
[15] M. Hubenthal, *An inverse source problem in radiative transfer with partial data*, Inverse Problems, 27 (2011), 125009.
[16] N. I. Ioakimidis, *A remark on singular integral equations with generalized kernels*, SIAM J. Appl. Math., 44 (1984), pp. 1106–1111, https://doi.org/10.1137/0144079.
[17] G. Jameson, *Hilbert's Inequality and Related Results*, https://www.maths.lancs.ac.uk/~jameson/hilbert.pdf; last accessed 5 July 2022.
[18] A. D. Kim and M. Moscoso, *Radiative transport theory for optical molecular imaging*, Inverse Problems, 22 (2005), pp. 23–42.
[19] F. W. King, *Hilbert Transforms*, Vol. 1, Encyclopedia Math. Appl. 124, Cambridge University Press, Cambridge, 2009.
[20] A. D. Klose, V. Ntziachristos, and A. H. Hielscher, *The inverse source problem based on the radiative transfer equation in optical molecular imaging*, J. Comput. Phys., 202 (2005), pp. 323–345.
[21] W. Koppelman and J. D. Pincus, *Spectral representations for finite Hilbert transformations*, Math. Z., 71 (1959), pp. 399–407.
[22] K. Matthews, *Hilbert's Inequality*, http://www.numbertheory.org/PDFS/hilbert.pdf; last accessed 5 July 2022.
[23] K. Matthews, *An Investigation of the Davenport-Halberstam Inequality and a Generalization of Artin's Conjecture for Primitive Roots*, Ph.D. thesis, University of Queensland, Queensland, Australia, 1974.
[24] N. I. Muskhelishvili, *Singular Integral Equations*, Dover Publications, Mineola, New York, 1992.
[25] F. Natterer, *The Mathematics of Computerized Tomography*, John Wiley & Sons, Chichester, UK, 1986.
[26] S. Okada and D. Elliott, *The finite Hilbert transform in $\mathscr{L}^2$*, Math Nachr., 153 (1991), pp. 43–56.
[27] K. Sadiq, O. Scherzer, and A. Tamasan, *On the X-ray transform of planar symmetric 2-tensors*, J. Math. Anal. Appl., 442 (2016), pp. 31–49.
[28] K. Sadiq and A. Tamasan, *On the range of the attenuated radon transform in strictly convex sets*, Trans. Amer. Math. Soc., 367 (2015), pp. 5375–5398.
[29] V. A. Sharafutdinov, *The inverse problem of determining the source in the stationary transport equation on a Riemannian manifold*, J. Math. Sci., 96 (1999), pp. 3430–3433.
[30] A. V. Smirnov, M. V. Klibanov, and L. H. Nguyen, *On an inverse source problem for the full radiative transfer equation with incomplete data*, SIAM J. Sci. Comput., 41 (2019), pp. B929–B952, https://doi.org/10.1137/19M1253605.
[31] P. Stefanov and G. Uhlmann, *An inverse source problem in optical molecular imaging*, Anal. PDE, 1 (2008), pp. 115–126.
[32] H. Takahasi and M. Mori, *Double exponential formulas for numerical integration*, Pub. Res. Inst. Math. Sci., 9 (1974), pp. 721–741.

[33] F. G. Tricomi, *Integral Equations*, Dover Publications, Mineola, New York, 1985, reprint of the 1957 original.
[34] I. N. Vekua, *Generalized Analytic Functions*, Pergamon Press, London, Paris, Frankfurt; Addison-Wesley, Reading, MA, 1962.
[35] H. Widom, *Singular integral equations in L_p*, Trans. Amer. Math. Soc., 97 (1960), pp. 131–160.